Core–Shell Nanostructures

Deutsche Ausgabe: DOI: 10.1002/ange.201500993
Internationale Ausgabe: DOI: 10.1002/anie.201500993

Synthesis of Ultrathin Face-Centered-Cubic Au@Pt and Au@Pd Core–Shell Nanoplates from Hexagonal-Close-Packed Au Square Sheets**

*Zhanxi Fan, Yihan Zhu, Xiao Huang, Yu Han, Qingxiao Wang, Qing Liu, Ying Huang, Chee Lip Gan, and Hua Zhang**

Abstract: *The synthesis of ultrathin face-centered-cubic (fcc) Au@Pt rhombic nanoplates is reported through the epitaxial growth of Pt on hexagonal-close-packed (hcp) Au square sheets (AuSSs). The Pt-layer growth results in a hcp-to-fcc phase transformation of the AuSSs under ambient conditions. Interestingly, the obtained fcc Au@Pt rhombic nanoplates demonstrate a unique $(101)_f$ orientation with the same atomic arrangement extending from the Au core to the Pt shell. Importantly, this method can be extended to the epitaxial growth of Pd on hcp AuSSs, resulting in the unprecedented formation of fcc Au@Pd rhombic nanoplates with $(101)_f$ orientation. Additionally, a small amount of fcc $(100)_f$-oriented Au@Pt and Au@Pd square nanoplates are obtained with the Au@Pt and Au@Pd rhombic nanoplates, respectively. We believe that these findings will shed new light on the synthesis of novel noble bimetallic nanostructures.*

Noble-metal nanocrystals (NCs) have attracted significant attention as they exhibit fascinating optical and catalytic properties and have shown potential applications in surface-enhanced Raman spectroscopy (SERS),[1] plasmonics,[1b] photothermal therapy,[2] and catalysis.[2,3] It has been established that the properties of noble-metal NCs can be tuned by their size and shape.[1a,2,3] More importantly, their functionalities are greatly affected by their crystal structures.[4] For example, the hexagonal-close-packed (hcp) Ag nanowire exhibited low-frequency electrical noise of two to six orders of magnitude lower than that of the conventional face-centered-cubic (fcc) Ag nanowire.[4a] Therefore, control of the crystal structure is critically important during the synthesis of noble-metal NCs. Previous efforts towards the structural manipulation of noble-metal NCs largely required extreme experimental conditions, such as high temperature,[5] high pressure,[6] or electron-beam irradiation under high-vacuum conditions.[7] However, the challenge remains to perform the structural modulation of noble-metal NCs under ambient conditions.

Over the last decade, much attention has been paid to the synthesis of binary noble-metal NCs as they display superior properties[8] and show much higher stability[8a,9] compared to their monometallic counterparts. Epitaxial growth has been commonly observed in the solution-phase synthesis of noble bimetallic NCs under ambient conditions because of the small lattice mismatch between the two metals (ordinarily $< 5\,\%$).[10] Typical synthetic procedures starts with metal NCs as the seeds, followed by successive epitaxial depositions[11] or Galvanic replacement reactions[12] with a secondary noble metal. To date, metal NCs with the shape of spheres,[13] nanorods,[12] triangular and hexagonal nanoplates,[9,14] or nanopolyhedra[10,11,15] have been used as seeds to synthesize bimetallic architectures with well-defined size, shape, composition, and atomic distribution (e.g., alloy, core–shell, or heterostructures). However, all of the seeds used in these works are in the fcc phase. Until now, the epitaxial growth of noble bimetallic NCs by using non-fcc nanocrystals as seeds has been rarely investigated,[16] especially for Au, Ag, Pt, and Pd.

In 2011, our group demonstrated the successful synthesis of pure hcp Au square sheets (AuSSs) on graphene oxide (GO).[7] Recently, we found that surface ligand exchange or deposition of Ag on the AuSS can induce its phase transformation from hcp to fcc.[17] Herein, for the first time we report the synthesis of ultrathin bimetallic fcc Au@Pt and Au@Pd core–shell nanoplates through the epitaxial growth of Pt and Pd on hcp AuSSs under ambient conditions. Interestingly, the obtained fcc Au@Pt and Au@Pd nanoplates show rhombic morphology and a unique $(101)_f$ orientation. A small amount of fcc $(100)_f$-oriented Au@Pt and Au@Pd square nanoplates coexist in their respective rhombic nanoplates. Our work demonstrates the many possibilities to prepare

[*] Z. Fan, Dr. X. Huang, Y. Huang, Prof. C. L. Gan, Prof. H. Zhang
School of Materials Science and Engineering
Nanyang Technological University
50 Nanyang Avenue, Singapore 639798 (Singapore)
E-mail: HZhang@ntu.edu.sg
Homepage: http://www.ntu.edu.sg/home/hzhang/
Y. Zhu, Prof. Y. Han
Advanced Membranes and Porous Materials Center
Physical Sciences and Engineering Division
King Abdullah University of Science and Technology
Thuwal 23955-6900 (Saudi Arabia)
Q. Wang
Imaging and Characterization Core Lab
King Abdullah University of Science and Technology
Thuwal 23955-6900 (Saudi Arabia)
Dr. Q. Liu
Nanyang Technological University
Temasek Laboratories@NTU, 9th Storey, BorderX Block
Research Techno Plaza 50 Nanyang Drive, 637553 (Singapore)

[**] This work was supported by MOE under AcRF Tier 2 (ARC 26/13, No. MOE2013-T2-1-034), AcRF Tier 1 (RG 61/12, RGT18/13, and RG5/13), and Start-Up Grant (M4080865.070.706022).

Supporting information for this article is available on the WWW under http://dx.doi.org/10.1002/anie.201500933.

bimetallic nanostructures based on the phase transformation of nanomaterials with ultra-small dimensions.

In a typical experiment, hcp AuSSs were synthesized according to our previous method with a slight modification (see the Experimental Section in the Supporting Information for details).[7] A representative transmission electron microscopy (TEM) image of the obtained hcp AuSSs is shown in Figure S1a in the Supporting Information. The as-prepared hcp AuSSs have an edge length of 100–400 nm (Figure S1a) and a thickness of 1.8 ± 0.5 nm (Figure S2a). The hcp structure of AuSSs is confirmed by the selected area electron diffraction (SAED) pattern taken along the $[110]_h$ zone axis (Figure S1b), which is consistent with our previous report.[7] In the following experiments, the obtained hcp AuSSs were used as seeds for the synthesis of bimetallic Au@Pt rhombic nanoplates.

The bimetallic Au@Pt nanoplates were synthesized by reduction of H_2PtCl_6 with $NaBH_4$ in the presence of hcp AuSSs (see the Experimental Section for details). Interestingly, the square-shaped AuSSs transformed to the rhombic nanoplates after coating with platinum (Figure 1a and Figure S3). The thickness of Au@Pt rhombic nanoplates is estimated to be 3.5 ± 0.7 nm by measuring their folded edges in the TEM image (Figure S2b). Strikingly, the electron-diffraction analysis indicates that the crystal structure of Au@Pt rhombic nanoplates is fcc with a unique $(101)_f$ orientation. In contrast to our result, almost all of the previously reported 2D fcc noble-metal nanostructures show a common $(111)_f$ orientation.[1a,9,14,18,19] The SAED patterns taken along the $[101]_f$ zone axis of typical fcc Au@Pt rhombic nanoplates are shown in Figure 1b and Figure S3. Diffraction spots derived from twinning are also detected and are marked with a subscript "T" (Figure 1b). The dark-field TEM (DF-TEM) image collected with the $(1\bar{1}\bar{1})_f$ reflection further reveals that the twinning is randomly distributed over the entire fcc Au@Pt rhombic nanoplate (Figure S4). The high-resolution TEM (HRTEM) images of a typical fcc Au@Pt rhombic nanoplate taken in the center and at the edges, respectively, are shown in Figure 1c,d. A lattice spacing of 2.3 Å is measured along the long diagonal of the Au@Pt rhombic nanoplate, which is attributed to the fcc {111} planes. The HRTEM images also clearly show the twinned structure, consistent with both the SAED and DF-TEM results (Figure 1b and Figure S4). The composition of such Au@Pt rhombic nanoplates is revealed from the STEM–EDS spectrum (Figure S5; STEM–EDS = scanning TEM–energy dispersive X-ray spectroscopy), which shows that the average Au to Pt atomic ratio is 1:1. The high-angle annular dark-field STEM (HAADF-STEM) image of a typical fcc Au@Pt rhombic nanoplate and the corresponding STEM–EDS elemental mapping clearly demonstrate that both Au and Pt atoms are homogeneously distributed in the as-prepared bimetallic Au@Pt rhombic nanoplates (Figure 1e–g), which is further corroborated by the STEM–EDS line scanning across the fcc Au@Pt rhombic nanoplate (Figure S6).

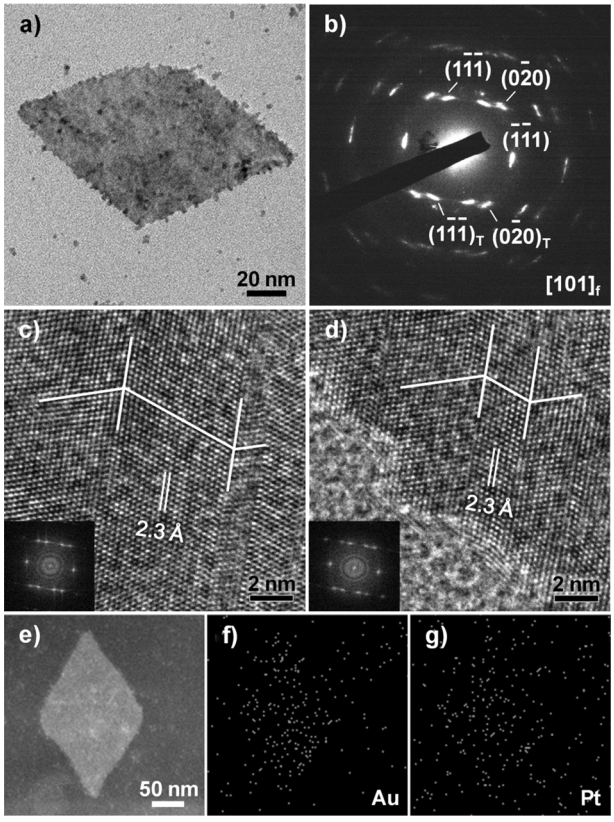

Figure 1. a) Bright-field TEM image and b) the corresponding SAED pattern of a typical fcc Au@Pt rhombic nanoplate with $(101)_f$ orientation. c,d) Typical HRTEM images of fcc Au@Pt rhombic nanoplates taken in the center and at the edges, respectively. Insets in (c,d): the corresponding FFT patterns for HRTEM images shown in (c) and (d). e) HAADF-STEM image and f,g) the corresponding STEM-EDS elemental mapping of a typical fcc (101)-oriented Au@Pt rhombic nanoplate.

To further investigate the structure of the fcc Au@Pt rhombic nanoplates, a focused ion beam (FIB) was utilized to cut it along the long diagonal (see Figure S7 and the Experimental Section in the Supporting Information for details), to reveal its cross-section (Figure 2a,b, and d). The corresponding STEM–EDS elemental mapping and line scanning of the cross-section indicate that a Pt layer covers the entire surface of the fcc Au nanosheets, resulting in a core–shell architecture (Figure 2e and f), which is further confirmed by STEM–EDS analysis at a selected point (Figure S8). The aberration-corrected high-resolution HAADF-STEM image of the cross-section fcc Au@Pt rhombic nanoplate shows continuous lattice fringes from the Au core to the Pt shell (Figure 2b), indicating the epitaxial relationship between the core and the shell. The lattice spacing of 2.3 Å corresponds to the fcc {111} planes of Au@Pt rhombic nanoplates. The corresponding fast Fourier transformation (FFT) pattern matches well with the electron-diffraction pattern along the fcc $[\bar{1}21]$ zone axis (Figure 2c), which further demonstrates the successful phase transformation of AuSSs from hcp to fcc.

Interestingly, in addition to the prepared fcc Au@Pt rhombic nanoplates, a small amount of Au@Pt square nanoplates (less than 10% yield) was also detected in the final products (Figure 3, Figure S9 and S10). Figure 3a shows the TEM image of a typical Au@Pt square nanoplate. Electron-diffraction analysis reveals that the obtained Au@Pt square

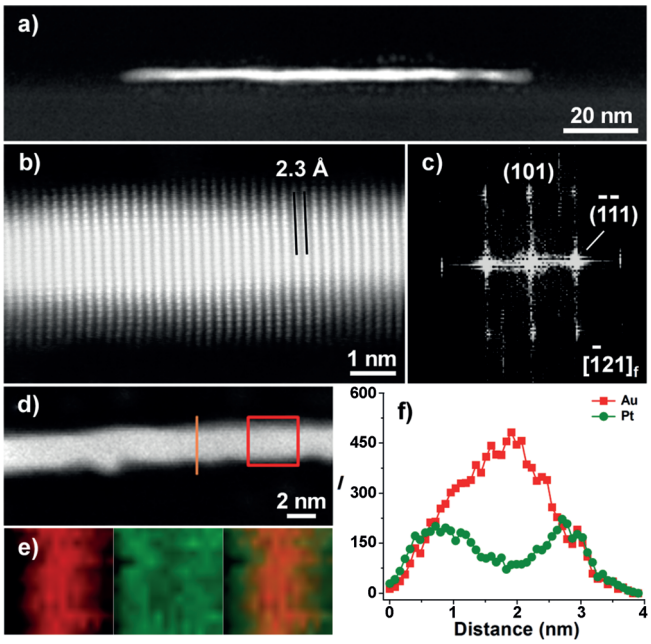

Figure 2. a) Low-magnification and b) aberration-corrected high-resolution HAADF-STEM images of the cross-section of an fcc Au@Pt rhombic nanoplate. c) The corresponding FFT pattern for the high-resolution HAADF-STEM image shown in (b). d) High-magnification HAADF-STEM image of the cross-section of the fcc Au@Pt rhombic nanoplate. e) The STEM-EDS elemental mappings of Au (left, red) and Pt (middle, green) and the overlapped image (right) from the selected rectangular area indicated in (d). f) The line-scanning profiles measured at the line indicated in (d).

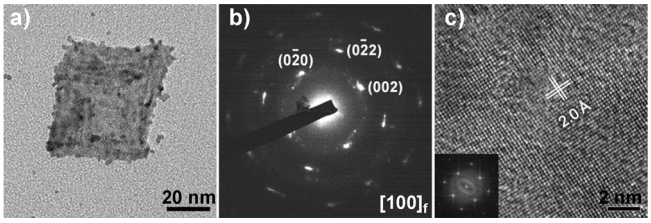

Figure 3. a) Bright-field TEM image and b) the corresponding SAED pattern of a typical fcc Au@Pt square nanoplate with $(100)_f$ orientation. c) Typical HRTEM image of a fcc Au@Pt square nanoplate. Scale bar = 2 nm. Inset in (c): the corresponding FFT pattern for the HRTEM image shown in (c).

nanoplate exhibits an fcc structure with a $(100)_f$ orientation, which is further identified by the corresponding HRTEM image (Figure 3b and c). The measured lattice spacing of 2.0 Å is attributed to the fcc {200} planes (Figure 3c).

Figure 4 (top-right panel) shows the phase and morphology transformation of hcp AuSSs induced by the overgrowth of an epitaxial Pt layer, that is, the transition of the original $(110)_h$-oriented hcp AuSSs to the unprecedented $(101)_f$-oriented fcc Au@Pt rhombic nanoplates. The hcp and fcc polymorphs differ in the stacking sequence of close-packed planes with repeated AB stacking along the $[001]_h$ direction and ABC stacking along the $[111]_f$ direction, respectively. This type of phase transformation can be

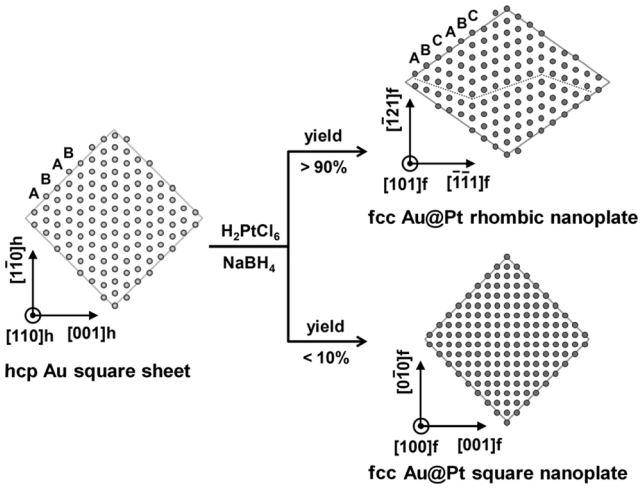

Figure 4. Schematic illustration of the synthesis of $(101)_f$-oriented fcc Au@Pt rhombic nanoplates with twinning (marked by the dashed line) from hcp Au square sheets (top panel). A small amount of $(100)_f$-oriented fcc Au@Pt square nanoplates (bottom panel) were also formed.

achieved through the variation of the stacking sequences of close-packed planes, resulting in the formation of lattice imperfections (e.g. twinning and stacking faults) and shape changes.[20] Moreover, the orientation of nanostructures relative to their close-packed directions (i.e. $[001]_h$ and $[111]_f$ directions) remains unchanged,[7,20c] which is consistent with our experimental results (Figure 1 and Figure S3). In contrast, the close-packed directions (i.e. $[001]_h$ and $[111]_f$ directions) changed during the phase transformation of $(110)_h$-oriented hcp AuSSs to $(100)_f$-oriented fcc Au@Pt square nanoplates (Figure 4, bottom-right panel).

Experimental and theoretical studies have indicated that the crystal structure of inorganic NCs is significantly affected by the surface energy, which contributes considerably to the total systemic energy.[7,20c,21] For instance, fcc Ru[4b] and hcp Ag[5,21b] nanoparticles have been synthesized although their bulk counterparts have hcp and fcc structures, respectively. In our work, the deposition of Pt on hcp AuSSs increased their thickness (Figure 2 and Figure S2b) and in turn decreased the surface area to volume ratio, which might partly lead to the instability of the original hcp structure and thus the transformation from hcp to fcc configurations.

Meanwhile, it has been well documented that epitaxial strain, caused by the lattice mismatch between the epitaxial thin film and the underlying substrate, plays a critical role in the final crystal structure of deposited thin films.[20a,22] In 2007, a study also showed that for spherical CdS@ZnS core–shell nanoparticles with a shell thickness of only 7.5 monolayers of ZnS, a 7% lattice mismatch between the core and shell generated a radial pressure of up to 4 GPa on the core.[23] In our work, the lattice mismatch between the close-packed planes of the hcp Au core ($\{001\}_h$ plane, $d = 2.4$ Å[7]) and the fcc Pt shell ($\{111\}_f$ plane, $d = 2.26$ Å, crystallography open database (COD) number 9013417) is about 5.8%. Note that the thickness of hcp AuSSs is only approximately 1.8 nm (Figure S2a), that is, approximately 12 Au atom layers.

Therefore, the effect of epitaxial strain imposed by the Pt shell on the structure of hcp AuSSs might be significant. Additionally, it has been suggested that the energy difference among the hcp, fcc, and body-centered-cubic (bcc) structures is quite small in many transition and noble metals.[24] Based on the above discussion, we speculate that the phase transformation of hcp AuSSs induced by the epitaxial growth of a Pt shell is most likely a result of the interplay between the surface energy, epitaxial strain, and phase stability. The reason for the coexistence of two kinds of phase transformations induced by the Pt coating on hcp AuSSs, that is, $(110)_h$-oriented hcp to $(101)_f$- and $(100)_f$-oriented fcc, remains elusive, and is still under investigation.

Importantly, the method reported herein is quite general. In addition to the use of a Pt coating as a shell for the Au core, the coating of Pd on hcp AuSSs can also induce the phase transformation of hcp AuSSs, resulting in the formation of fcc Au@Pd rhombic nanoplates (Figure 5 and Figure S11). The fcc structure of Au@Pd rhombic nanoplates is suggested by the SAED pattern with twinning (Figure 5b), which are corroborated by the dark-field TEM image collected in the $(1\bar{1}\bar{1})_f$ reflection (Figure S12). The typical HRTEM images taken perpendicular to the basal surface of Au@Pd rhombic nanoplates further reveal the occurrence of twinning and a unique $(101)_f$ orientation (Figure 5c and d). The thickness of fcc Au@Pd rhombic nanoplates is estimated to be 3.4 ± 0.8 nm by measuring the folded Au@Pd rhombic nanoplates (Figure S2c). Quantitative STEM–EDS analysis indicates the presence of Au and Pd atoms (Figure S13) with an average atomic ratio of 1:0.8 (Au:Pt). The HAADF-STEM image of a typical fcc Au@Pd rhombic nanoplate is shown in Figure 5e. The corresponding STEM–EDS elemental mapping (Figure 5f and g) reveals that both Au and Pd are uniformly distributed in the fcc Au@Pd rhombic nanoplate, which is further verified by the STEM–EDS line scanning across the fcc Au@Pd rhombic nanoplate (Figure S14). Additionally, a small amount of $(100)_f$-oriented fcc Au@Pd square nanoplates with a yield of less than 10% was also found in the final product (Figure S15 and S16), which is similar to the result described above for Pt deposition on hcp AuSSs (Figure 3).

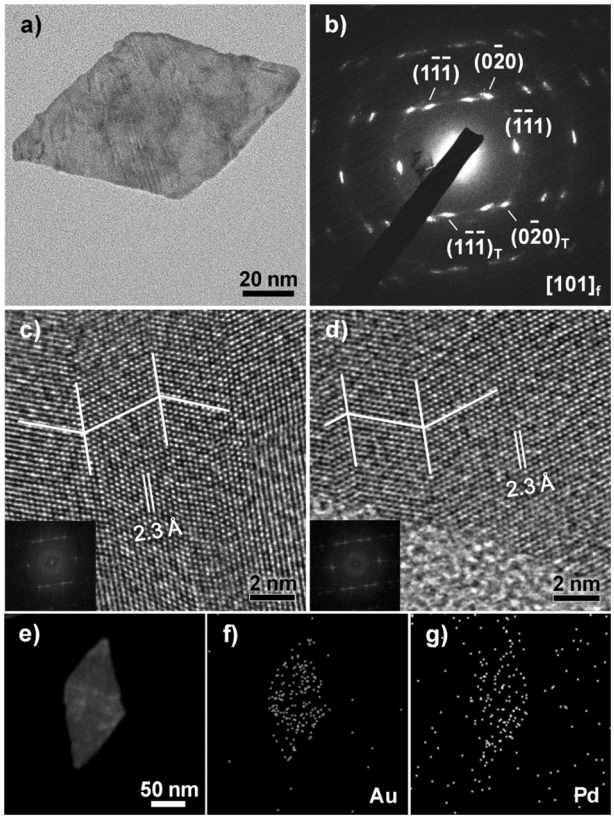

Figure 5. a) Bright-field TEM image and b) the corresponding SAED pattern of a typical fcc Au@Pd rhombic nanoplate with $(101)_f$ orientation. c, d) HRTEM images of the fcc Au@Pd rhombic nanoplate taken in the center and at the edges, respectively. Insets in (c, d): the corresponding FFT patterns of HRTEM images in (c, d). e) HAADF-STEM image and f, g) the corresponding STEM–EDS elemental mapping of a typical fcc $(101)_f$-oriented Au@Pd rhombic nanoplate.

In summary, we have successfully synthesized for the first time ultrathin fcc (101)-oriented Au@Pt core–shell rhombic nanoplates through the epitaxial growth of Pt on hcp AuSSs under ambient conditions. A number of stacking faults and internal twinning were produced in the obtained fcc Au@Pt rhombic nanoplates. Importantly, this method for the simultaneous phase transformation and formation of core–shell bimetallic structures can be extended to the synthesis of fcc (101)-oriented Au@Pd rhombic nanoplates. Interestingly, a small amount of fcc (100)-oriented Au@Pt and Au@Pd square nanoplates were also prepared with the major products of fcc (101)-oriented Au@Pt and Au@Pd rhombic nanoplates. We believe that the rational control of the structure, shape, and composition of bimetallic nanostructures in this work will pave the way towards the design and synthesis of advanced bimetallic nanomaterials with potential applications in SERS, plasmonics, and catalysis.

Keywords: electron microscopy · gold · nanostructures · noble metals · phase transformation

How to cite: *Angew. Chem. Int. Ed.* **2015**, *54*, 5672–5676
Angew. Chem. **2015**, *127*, 5764–5768

[1] a) Y. Xia, Y. Xiong, B. Lim, S. E. Skrabalak, *Angew. Chem. Int. Ed.* **2009**, *48*, 60–103; *Angew. Chem.* **2009**, *121*, 62–108; b) N. J. Halas, S. Lal, W.-S. Chang, S. Link, P. Nordlander, *Chem. Rev.* **2011**, *111*, 3913–3961; c) M. R. Jones, K. D. Osberg, R. J. Macfarlane, M. R. Langille, C. A. Mirkin, *Chem. Rev.* **2011**, *111*, 3736–3827.

[2] X. Huang, S. Tang, X. Mu, Y. Dai, G. Chen, Z. Zhou, F. Ruan, Z. Yang, N. Zheng, *Nat. Nanotechnol.* **2011**, *6*, 28–32.

[3] N. Tian, Z.-Y. Zhou, S.-G. Sun, Y. Ding, Z. L. Wang, *Science* **2007**, *316*, 732–735.

[4] a) A. Singh, T. P. Sai, A. Ghosh, *Appl. Phys. Lett.* **2008**, *93*, 102107; b) K. Kusada, H. Kobayashi, T. Yamamoto, S. Matsumura, N. Sumi, K. Sato, K. Nagaoka, Y. Kubota, H. Kitagawa, *J. Am. Chem. Soc.* **2013**, *135*, 5493–5496.

[5] P. Taneja, R. Banerjee, P. Ayyub, G. K. Dey, *Phys. Rev. B* **2001**, *64*, 033405.

[6] Y. Sun, W. Yang, Y. Ren, L. Wang, C. Lei, *Small* **2011**, *7*, 606–611.

[7] X. Huang, S. Li, Y. Huang, S. Wu, X. Zhou, C. L. Gan, F. Boey, C. A. Mirkin, H. Zhang, *Nat. Commun.* **2011**, *2*, 292.

[8] a) J. Zhang, K. Sasaki, E. Sutter, R. R. Adzic, *Science* **2007**, *315*, 220–222; b) B. Lim, M. Jiang, P. H. Camargo, E. C. Cho, J. Tao,

X. Lu, Y. Zhu, Y. Xia, *Science* **2009**, *324*, 1302 – 1305; c) J. Wu, P. Li, Y.-T. Pan, S. Warren, X. Yin, H. Yang, *Chem. Soc. Rev.* **2012**, *41*, 8066 – 8074; d) J. Gu, Y.-W. Zhang, F. Tao, *Chem. Soc. Rev.* **2012**, *41*, 8050 – 8065; e) X. Liu, D. Wang, Y. Li, *Nano Today* **2012**, *7*, 448 – 466.

[9] C. Gao, Z. Lu, Y. Liu, Q. Zhang, M. Chi, Q. Cheng, Y. Yin, *Angew. Chem. Int. Ed.* **2012**, *51*, 5629 – 5633; *Angew. Chem.* **2012**, *124*, 5727 – 5731.

[10] F.-R. Fan, D.-Y. Liu, Y.-F. Wu, S. Duan, Z.-X. Xie, Z.-Y. Jiang, Z.-Q. Tian, *J. Am. Chem. Soc.* **2008**, *130*, 6949 – 6951.

[11] a) C.-L. Lu, K. S. Prasad, H.-L. Wu, J.-a. A. Ho, M. H. Huang, *J. Am. Chem. Soc.* **2010**, *132*, 14546 – 14553; b) J. Zeng, C. Zhu, J. Tao, M. Jin, H. Zhang, Z. Y. Li, Y. Zhu, Y. Xia, *Angew. Chem. Int. Ed.* **2012**, *51*, 2354 – 2358; *Angew. Chem.* **2012**, *124*, 2404 – 2408; c) S. E. Habas, H. Lee, V. Radmilovic, G. A. Somorjai, P. Yang, *Nat. Mater.* **2007**, *6*, 692 – 697.

[12] P. H. C. Camargo, Y. Xiong, L. Ji, J. M. Zuo, Y. Xia, *J. Am. Chem. Soc.* **2007**, *129*, 15452 – 15453.

[13] a) J. Zhang, Y. Tang, L. Weng, M. Ouyang, *Nano Lett.* **2009**, *9*, 4061 – 4065; b) M. R. Langille, J. Zhang, M. L. Personick, S. Li, C. A. Mirkin, *Science* **2012**, *337*, 954 – 957.

[14] B. Lim, J. Wang, P. H. C. Camargo, M. Jiang, M. J. Kim, Y. Xia, *Nano Lett.* **2008**, *8*, 2535 – 2540.

[15] a) F. Wang, C. Li, L. D. Sun, H. Wu, T. Ming, J. Wang, J. C. Yu, C. H. Yan, *J. Am. Chem. Soc.* **2011**, *133*, 1106 – 1111; b) J. W. Hong, D. Kim, Y. W. Lee, M. Kim, S. W. Kang, S. W. Han, *Angew. Chem. Int. Ed.* **2011**, *50*, 8876 – 8880; *Angew. Chem.* **2011**, *123*, 9038 – 9042.

[16] Y.-C. Hsieh, Y. Zhang, D. Su, V. Volkov, R. Si, L. Wu, Y. Zhu, W. An, P. Liu, P. He, S. Ye, R. R. Adzic, J. X. Wang, *Nat. Commun.* **2013**, *4*, 2466.

[17] Z. Fan, X. Huang, Y. Han, M. Bosman, Q. Wang, Y. Zhu, Q. Liu, B. Li, Z. Zeng, J. Wu, W. Shi, S. Li, C. L. Gan, H. Zhang, *Nat. Commun.* **2015**, *6*, 6571.

[18] X. Sun, S. Dong, E. Wang, *Angew. Chem. Int. Ed.* **2004**, *43*, 6360 – 6363; *Angew. Chem.* **2004**, *116*, 6520 – 6523.

[19] J. Turkevich, P. C. Stevenson, J. Hillier, *Discuss. Faraday Soc.* **1951**, *11*, 55 – 75.

[20] a) W. Tian, H. P. Sun, X. Q. Pan, J. H. Yu, M. Yeadon, C. B. Boothroyd, Y. P. Feng, R. A. Lukaszew, R. Clarke, *Appl. Phys. Lett.* **2005**, *86*, 131915; b) K. Jacobs, D. Zaziski, E. C. Scher, A. B. Herhold, A. P. Alivisatos, *Science* **2001**, *293*, 1803 – 1806; c) X. Huang, H. Li, S. Li, S. Wu, F. Boey, J. Ma, H. Zhang, *Angew. Chem. Int. Ed.* **2011**, *50*, 12245 – 12248; *Angew. Chem.* **2011**, *123*, 12453 – 12456.

[21] a) J. M. McHale, *Science* **1997**, *277*, 788 – 791; b) X. Liu, J. Luo, J. Zhu, *Nano Lett.* **2006**, *6*, 408 – 412.

[22] R. J. Zeches, M. D. Rossell, J. X. Zhang, A. J. Hatt, Q. He, C. H. Yang, A. Kumar, C. H. Wang, A. Melville, C. Adamo, G. Sheng, Y. H. Chu, J. F. Ihlefeld, R. Erni, C. Ederer, V. Gopalan, L. Q. Chen, D. G. Schlom, N. A. Spaldin, L. W. Martin, R. Ramesh, *Science* **2009**, *326*, 977 – 980.

[23] S. Ithurria, P. Guyot-Sionnest, B. Mahler, B. Dubertret, *Phys. Rev. Lett.* **2007**, *99*, 265501.

[24] H. L. Skriver, *Phys. Rev. B* **1985**, *31*, 1909 – 1923.

Received: February 2, 2015
Published online: March 17, 2015

